Correlation Study of Temporal and Emission Properties of Quiescent Magnetars

Jiwoo Seo [1], **Jaewon Lee** [1,2], **and Hongjun An** [1,★]

[1] Department of Astronomy and Space Science, Chungbuk National University, Cheongju 28644, Republic of Korea
[2] METASPACE, Cheongju 28156, Republic of Korea
★Corresponding Author: H. An, hjan@cbnu.ac.kr

Abstract

We measured temporal and emission properties of quiescent magnetars using archival Chandra and XMM-Newton data, produced a list of the properties for 17 magnetars, and revisited previously suggested correlations between the properties. Our studies carried out with a larger sample, better spectral characterizations, and more thorough analyses not only confirmed previously-suggested correlations but also found new ones. The observed correlations differ from those seen in other neutron-star populations but generally accord with magnetar models. Specifically, the trends of the intriguing correlations of blackbody luminosity (L_{BB}) with the spin-inferred dipole magnetic field strength (B_S) and characteristic age (τ_c) were measured to be $L_{BB} \propto B_S^{1.5}$ and $L_{BB} \propto \tau_c^{-0.6}$, supporting the twisted magnetosphere and magnetothermal evolution models for magnetars. We report the analysis results and discuss our findings in the context of magnetar models.

Keywords: stars: neutron — stars: statistics — pulsars: general — X-rays

1. Introduction

Magnetars are neutron stars with an ultrastrong magnetic field (B), greater than the quantum critical threshold of 4.414×10^{13} G. They have relatively long spin periods ($P \sim 2$–12 s) and large spin-down rates ($\dot{P} \sim 10^{-13}$–10^{-10} s s^{-1}) compared to rotation-powered pulsars (RPPs). Thus magnetars have strong spin-inferred dipole magnetic-field strengths $B_S = 3.2 \times 10^{19}\sqrt{P\dot{P}}$ G of typically $>10^{14}$ G. Magnetars' emission is mostly in the X-ray band and is thought to be produced primarily by the decay of internal B (Thompson & Duncan 1995, 1996; Thompson et al. 2002). Thus, B is the key to understand observational properties of magnetars (e.g., as compared to RPPs). They are a source of fast radio bursts (FRBs) (e.g., CHIME/FRB Collaboration et al. 2020; Bochenek et al. 2020) and can be an important contributor to the gravitational wave (GW) background (e.g., Regimbau & de Freitas Pacheco 2006; Ho 2016). Hence it is very important to characterize and understand magnetars' properties well, especially in the advent of sensitive instruments for GW (LIGO Scientific Collaboration et al. 2015) and FRB detection (CHIME/FRB Collaboration et al. 2018).

The most distinctive features of magnetars' emission in comparison to RPPs' are bursts and outbursts (e.g., Kaspi et al. 2003; Coti Zelati et al. 2018) which occur in magnetars much more frequently than in RPPs (e.g., Perna & Pons 2011). The internal decay of B can be generated via ambipolar diffusion and Hall drift (e.g., Goldreich & Reisenegger 1992); these can apply stress to the stellar crust which may then be sheared. The crust displacement by the magnetic shear may twist external B and induce various instabilities in the magnetosphere (e.g., Beloborodov 2009). They generate diverse transient behaviors (e.g., Kaspi & Beloborodov 2017), e.g., bursts and outbursts. Magnetar bursts on a timescale of seconds may be produced by rapid magnetospheric reconnection in the magnetosphere (e.g., Lyutikov 2003), and outbursts are suggested to be caused by changes in the global B structure (e.g., Beloborodov & Thompson 2007). These transient phenomena have been used to test magnetar models and helped to refine them.

Quiescent emissions of magnetars reflect their persistent properties and can also provide important clues to magnetar physics (e.g., Kaspi & Boydstun 2010). Quiescent X-ray spectra of magnetars are well characterized with thermal blackbody radiation from the surface and/or nonthermal radiation in the magnetosphere, and modulate on the spin periods. These observed emission properties are similar to those of other X-ray pulsars, but there are differences; (1) surface temperatures of magnetars are inferred to be higher than those of other X-ray pulsars, and (2) the spectral energy distributions of the nonthermal emissions from some magnetars show a dramatic

turn-over at ~10 keV (Kuiper et al. 2006). Both of them are thought to be caused by the strong B of magnetars. (1) can be explained as due to the power supplied by the internal B decay, and (2) may imply that the magnetospheric emission mechanism of magnetars is different from that of RPPs; magnetospheric emission of magnetars is thought to be produced by resonant cyclotron scattering (RCS) of the thermal photons by electrons in the twisted B field (e.g., Thompson et al. 2002; Lyutikov & Gavriil 2006; Pons et al. 2007; Beloborodov 2013; Wadiasingh et al. 2018) not by their synchrotron radiation as has been suggested for RPPs (e.g., Wang et al. 2013; Torres et al. 2019).

Although B is the key to understand the quiescent emission of magnetars, there may be other important factors. Spin-down power $\dot{E}_{SD} (\propto \dot{P}/P^3)$ may play a role for the emission, and spin-down torque ($\propto \dot{\nu}$) may be influenced by plasma surrounding the star. The emission strength and the physical parameters co-evolve on a timescale of ~Myr via a long-term decay of B due to conduction and diffusion (e.g., Pons et al. 2007; Viganò et al. 2013), and so the age (t_{age}) may also be an important factor. Impacts of these physical properties (B, t_{age} etc.) on the emission would be manifested by correlation between the physical and radiative properties; such correlations have been seen in populations of X-ray pulsars (e.g., Li et al. 2008; Zhu et al. 2011)

Statistical studies of quiescent properties of magnetars have been performed previously. Marsden & White (2001) reported a correlation between spin frequency derivative ($\dot{\nu}$; spin-down torque) and soft X-ray (0.5–10 keV) photon index (Γ). Kaspi & Boydstun (2010) used a larger sample and suggested that both soft-band (<10 keV) and hard-band (>10 keV) spectral indices are correlated with B_S. Enoto et al. (2010) found that spectral hardness (1–60 keV flux ratio of a hard and a soft spectral component) is correlated with the characteristic age (τ_c) and B_S. These helped to develop the twisted-B model (e.g., Thompson et al. 2002; Beloborodov 2013). An et al. (2012) found a correlation between B_S and 2–10 keV X-ray luminosity ($L_{2-10\ keV}$) using a sample of high-B pulsars and magnetars, and suggested that they share similar physical processes which are controlled primarily by B; this is in accord with the discoveries of low-B_S ($\lesssim 10^{13}$ G) magnetars (Rea et al. 2013) and magnetar-like outbursts in typical RPPs (e.g., Gavriil et al. 2008; Archibald et al. 2018). Mong & Ng (2018) confirmed the B_S-$L_{2-10\ keV}$ correlation. They further employed a two-blackbody (2BB) or two-blackbody plus power-law (2BB+PL) model for the spectra, and found that the cold BB temperature (kT_1) is correlated with B_S, lending supports to the long-term magnetothermal evolution models (e.g., Pons et al. 2007; Perna & Pons 2011; Viganò et al. 2013). Coti Zelati et al. (2018) compiled outburst and quiescent fluxes of magnetars, and performed a systematic study with emphasis on the outburst properties.

More magnetars have been discovered and their quiescent properties have been better measured since the previous correlation studies. Thus, it is timely to update the correlation results with a larger sample, refined measurements, and thorough analyses. In this paper, we carefully identified quiescent states of magnetars using information collected from literature, and selected 17 magnetars whose quiescent properties could be well characterized (Section 2). We measured their emission properties and investigated correlations between various radiative and temporal properties including pulsed fractions (η) (see Section 3.2 for the definition of η) which has not been investigated previously (Sections 3 and 4). We discussed the correlation results in Section 5, and summarized them in Section 6.

2. Target Selection and Data Reduction

We selected targets for our study based on the McGill online magnetar catalog[1] (Olausen & Kaspi 2014) and the magnetar outburst online catalog (Coti Zelati et al. 2018).[2] The former lists basic temporal and spectral properties of quiescent magnetars, and the latter provides long-term light curves and helps to identify the epoch of the faintest state for some magnetars. We made a further literature search to choose adequate observational data collected in quiescence, and analyzed them to measure the quiescent properties. While the previous measurements were useful, we reanalyzed the quiescent data because some of quantities we intended to investigate (e.g., BB radius, η and PL flux) could not be retrieved from the catalogs or literature. Note that the quiescent data used in this study were taken during one quiescent period, i.e., we did not combine data acquired before and after an outburst.

The targets and data used in this work are listed in Table 1. Note that the list is slightly different from that in the McGill or the outburst catalog because we omitted magnetars whose quiescent properties could not be measured. For most of the targets, the quiescent state was well identified by a period with stable and low flux. But low-cadence observations for some magnetars did not allow a firm identification of the 'stable' quiescent state, and for them we assumed that the lowest-flux data far away (>a few years) from their outbursts represent well the quiescent states.

We downloaded archival Chandra and XMM-Newton (XMM hereafter) data from the HEASARC data archive and reduced them following the standard procedures. We reprocessed the Chandra data using the `chandra_repro` tool of CIAO 4.13 along with CALDB 4.9.4. The XMM-Newton data were reduced with the `emproc` and `epproc` tasks of XMM science analysis system (SAS) v2019, and we filtered out particle flares from the data following the flare-removal procedure.[3] Note that there are Swift data available for some targets, but given the small effective area of the instrument and short exposures for the observations, the Swift data are less useful. Note also that Suzaku and NuSTAR observed a few targets, which can help our investigation. We discussed these measurements (Section 3.3) but did not use them in this study. We defer further Suzaku and NuSTAR investigations to future work.

---

[1] http://www.physics.mcgill.ca/~pulsar/magnetar/main.html
[2] http://magnetars.ice.csic.es/#/welcome
[3] https://www.cosmos.esa.int/web/xmm-newton/sas-thread-epic-filterbackground

Table 1. Spectral and temporal properties of the selected targets

#[a]	Obs ID	Inst.[b]	Model	N_H (10^{22} cm^{-2})	kT_1 (keV)	$R_{1,BB}$ (km)	kT_2 (keV)	$R_{2,BB}$ (km)	Γ	L_{PL} (10^{35} erg s^{-1})	P^c (s)	$\dot{P}^c$ (10^{-11})	η	ξ	d^c (10 kpc)	χ^2/dof	Net counts
1	0304250401	X	BB+PL	$0.091^{+0.079}_{-0.038}$	0.34(1)	9.6(6)	—	—	1.9(1)	0.7(1)	8.02	1.88	0.27(4)	2	6.24	109/97	3227(58)
2	0112781101	X	2BB+PL	0.70(2)	0.30(1)	13.8(6)	0.55(2)	3.0(3)	2.90(4)	1.4(1)	8.69	0.20	0.07(1)	2	0.36	140/131	163440(405)
3	0693100101	X	BB	0.115(6)	0.36(2)	0.06(1)	—	—	—	—	9.08	0.0004	0.65(9)	1	0.2	33/23	486(32)
4	14811,15564	C	BB+PL	1.4(1)	0.74(4)	0.10(2)	—	—	3.9(1)	0.058(2)	5.76	0.59	0.46(2)	3	0.2	261/280	8027(90)
5	10806	C	BB+PL	0.06/0.54(6)[d]	0.45(3)	7(1)	—	—	2.4(1)	5.6(4)	8.05	3.8	—	—	5.36	123/140	4200(66)
6	6736[e]	C	BB+PL	0.97(1)	0.57(1)	2.02(8)	—	—	3.0(1)	1.38(4)	6.46	2.25	0.68(1)	2	0.9	303/283	19768(141)
7	0402910101	X	BB+PL	3.46(3)	0.40(2)	0.8(2)	—	—	4.0(1)	$0.13^{+0.03}_{-0.02}$	2.07	4.77	—	—	0.45	140/131	4632(70)
8	0742650101	X	PL	10(2)	—	—	—	—	2.1(3)	0.02(1)	2.59	1.9	—	—	1.1	53/51	175(19)
9	0404340101	X	BB+PL	2.39(5)	0.56(5)	0.17(3)	—	—	3.8(2)	$0.039^{+0.006}_{-0.005}$	10.61	0.02	0.80(3)	1	0.39	129/136	2829(57)
10	4605[e]	C	BB+PL	1.36(4)	0.455(4)	3.3(1)	—	—	2.50(2)	1.42(3)	11.01	1.95	0.324(5)	3	0.38	479/440	120681(348)
11	0790870201	X	BB+PL	3.6(2)	0.61(1)	1.56(5)	—	—	0.9(4)	$0.12^{+0.03}_{-0.02}$	3.83	6.4	0.29(3)	1	1.32	234/203	8444(98)
12	0654230401	X	BB+PL	9.7(1)	0.59(3)	1.2(1)	—	—	1.4(1)	0.8(1)	7.55	49.5	0.06(2)	1	0.87	241/212	14252(121)
13	15870	C	2BB	0.92(2)	0.17(1)	10(1)	0.33(2)	0.9(2)	—	—	5.54	0.78	0.33(3)	1	0.35	71/89	3095(56)
14	15589–15593	C	BB+PL	0.453(8)	0.12(1)	4(1)	—	—	4.5(4)	$2^{+0.9}_{-0.6} \times 10^{-3}$	8.44	0.002	0.38(3)	1	0.16	128/114	2157(46)
15	0013340201	X	BB+PL	2.26(5)	0.41(1)	6.14(4)	—	—	2.25(6)	3.3(2)	11.79	4.09	0.15(2)	2	0.85	299/321	26306(168)
16	0790610101	X	BB+PL	1.9(1)	0.52(1)	2.6(1)	—	—	1.3(2)	0.38(4)	5.20	9.20	0.20(2)	2	1.25	278/237	12053(111)
17	0057540101	X	BB+PL	1.10(2)	0.48(2)	1.5(1)	—	—	4.03(5)	2.4(1)	6.98	0.05	0.18(1)	2	0.32	452/447	19715(141)

Numbers in parentheses are the statistical uncertainties at the 1σ level. [a] 1. CXOU J010043.1−721134, 2. 4U 0142+61, 3. SGR 0501+4516, 4. SGR 0418+5729, 5. SGR 0526−66, 6. 1E 1048.1−5937, 7. 1E 1547.0−5408, 8. SGR 1627−41, 9. CXOU J164710.2−455216, 10. 1RXS J170849.0−400910, 11. CXOU J171405.7−381031, 12. SGR 1806−20, 13. XTE J1810−197, 14. Swift J1822.3−1606, 15. 1E 1841−045, 16. SGR 1900+14, 17. 1E 2259+586. [b]Instrument. X: XMM and C: Chandra. [c]Values taken from the McGill online catalog. [d]Absorption column densities in the Galaxy and large Magellanic cloud (Park et al. 2012). [e]Continuous clocking mode observation.

3. Data Analysis Result

We describe general analysis procedure first (Sections 3.1 and 3.2) and present the results for each target in Section 3.3.

3.1. Spectral Analysis

Quiescent fluxes of magnetars substantially differ from source to source, and so we selected adequate source and background regions for each source for spectral analysis.

For the Chandra data, we used a $R = 1''$–$4.5''$ circular region centered at the source position to extract the source spectrum, and used a $R = 2''$–$10''$ circle in a nearby source-free region to extract the background spectrum. Note that we used $5'' \times 50''$ and $10'' \times 50''$ rectangular regions for the source and background extraction, respectively, for the bright magnetars 1E 1048.1−5937 and 1RXS J170849.0−400910 because the observations were taken with the continuous clocking mode (Table 1). For the XMM data analysis, we used a $R = 16''$–$20''$ and a $R = 40''$–$60''$ circle for the source and background extraction, respectively. The target 1E 2259+586 was observed far off-axis, and thus we used a $20'' \times 40''$ elliptical region for the source spectrum. We verified that the results did not alter significantly depending on the source/background region selections. Corresponding response files were generated with the standard CIAO and SAS tools for the Chandra and XMM data, respectively. We fit the spectra employing the χ^2 statistic after grouping them to have a minimum of 20 events per spectral bin except for SGR 1627−41. For it, we grouped the spectra to have at least 5 events per bin due to a lack of photon statistics and utilized the l statistic[4] (Loredo 1992) for the spectral fit.

Actual emission spectra of magnetars can be very complex to be fully described by simple phenomenological models because the thermal emission from the surface is modified in the atmosphere and magnetosphere (e.g., Ho & Lai 2001; Potekhin & Yakovlev 2001) and the nonthermal emission depends on the poorly known RCS geometry (e.g., Wadiasingh et al. 2018). In general, a BB, PL, or BB+PL model has been employed in literature because they can approximately represent the thermal and/or nonthermal emissions of magnetars. We adopted the BB+PL model as the default since it has been most commonly used in previous studies (Section 3.3). We checked to see if the model adequately describes our data, and made a literature search to see if a different model has been favored on statistical or physical grounds. The BB+PL model adequately described the spectra of most of the targets in the previous and our studies (Table 1). A different model, BB, PL, 2BB, or 2BB+PL, was favored for some targets (e.g., 4U 0142+61, SGR 0418+5729, SGR 1627−41, and XTE J1810−197; Table 1) in previous studies, and our investigation of their spectra agreed with the previous results; for these targets we adopted the favored models. Note also that multiple spectral models (mostly BB+PL and 2BB) could not be discerned for some magnetars. In these cases, we took the BB+PL model as our baseline and investigated the other model as an alternative in the correlation study (see Section 4.2).

---

[4] https://heasarc.gsfc.nasa.gov/xanadu/xspec/manual/XSappendixStatistics.html

We fit the source spectra with the aforementioned models in XSPEC v12.11.1 (Arnaud 1996) and show them in Figure 1. Because the absorption column densities (N_H) towards some targets were often not well constrained with the quiescent data alone due to the paucity of counts, we searched literature for N_H values that were inferred from a multi-epoch spectral analysis conducted with the same spectral model as ours. If such a value was available, we used the same abundance and cross section as those in the literature and held N_H fixed at the value (Section 3.3). If we could not find a reported value of N_H, we optimized it in our spectral fit using the tbabs model with vern cross section (Verner et al. 1996) and angr abundance (Anders & Grevesse 1989). The measured spectra and the best-fit parameters are presented in Figure 1 and Table 1, respectively. The models describe the data adequately (null hypothesis probabilities > 0.03) although some residuals are noticeable. They may indicate some other physical processes (e.g., cyclotron absorption; Tiengo et al. 2013) but an additional component was not required in the spectral fits. We describe the analysis results in more detail in Section 3.3.

3.2. Timing Analysis

In our measurements of the temporal properties of the quiescent magnetars, we attempted to detect their pulsations and measure P at the epoch. Even though they were already well measured (e.g., McGill magnetar catalog), our reanalyses were necessary because P changes with time (e.g., slowly due to $\dot{P}$) and would be different at the epoch of the observational data we analyzed. Small inaccuracies ($<10^{-2}$ s) in P are not a problem for our correlation study, but the measurements of η may be substantially affected by the inaccuracies.

For a timing analysis, we barycenter-corrected the source and background event arrival times using the source positions reported in the McGill magnetar catalog and searched for pulsations of each target by employing an H test (e.g., de Jager et al. 1989) to measure P of the target at the epoch of the observation. The pulsations were well detected for most of the targets except for a few faint sources. The measured P values are not very different ($\Delta P/P \leq 0.005$) from those reported in the McGill catalog. We then constructed pulse profiles of the source and background emissions by folding 0.5–10 keV events on the best period. The background-subtracted pulse profiles are displayed in Figure 2.

While η of a magnetar can be defined in various ways (e.g., Vogel et al. 2014; An et al. 2015), in this work we defined it to be the area fraction above the constant level in the pulse profiles which were modeled as a combination of Gaussian functions. We fit the profiles of the targets with a Gaussian plus constant function employing the χ^2 statistic and successively added more Gaussians until an additional Gaussian was unnecessary. For each addition of a Gaussian, we performed an F test. Note that the ideal F distribution may be inadequate in the case that the parameter values of the additional component are near their boundaries. Hence we carried out simulations (e.g., Protassov et al. 2002); we generated 10,000 fake profiles based on the simpler model, fit them with the more complex
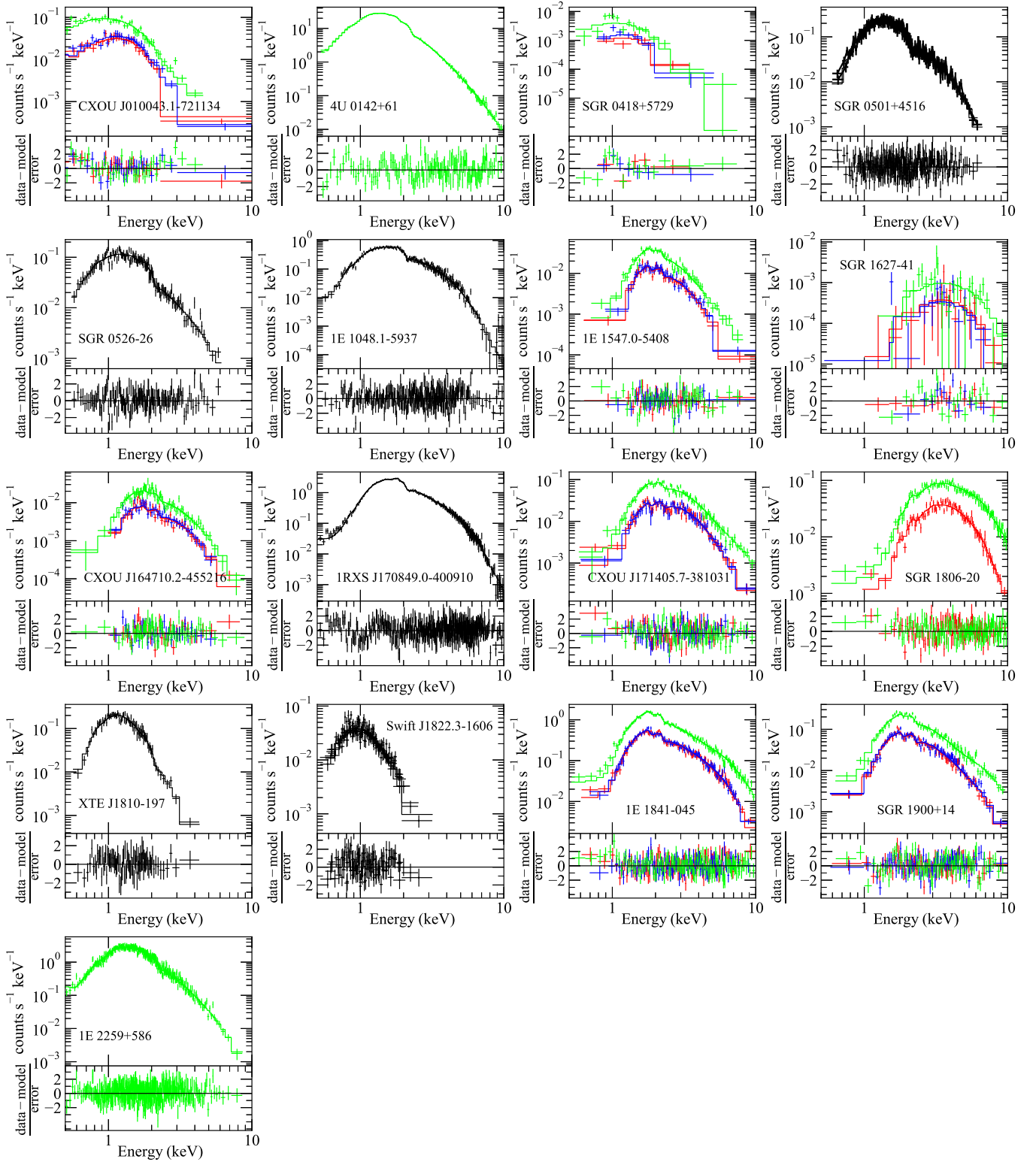
Figure 1. 0.5–10 keV quiescent spectra of the targets in Table 1. Chandra-measured spectra are plotted in black, and XMM-measured ones are shown in red (Mos1), blue (Mos2), and green (PN). The bottom panel in each figure shows residual after subtracting the best-fit model (solid lines).
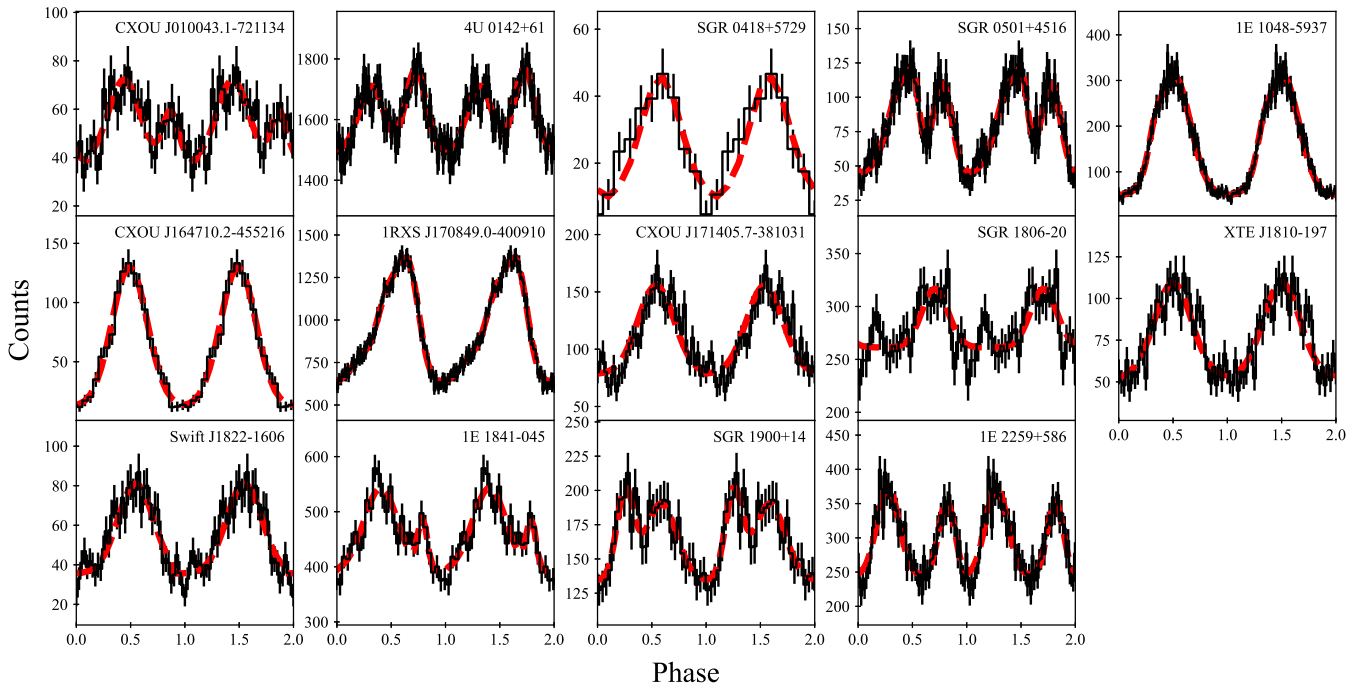
Figure 2. Background-subtracted 0.5–10 keV pulse profiles (black) of the targets of which pulsations were significantly detected. The best-fit models are displayed by red dashed lines.

model to compute the F values, and derived an F distribution appropriate for the model comparison. We required the p value corresponding to the measured F to be less than 0.01 for an addition of a new component. We verified that the optimized models achieved good fits to the pulse profiles with the χ^2 probabilities > 0.2. The numbers of Gaussians (ξ) needed to fit the profile and the estimated η are presented in Table 1. We further verified the ξ values using the unbinned likelihood fit and Akaike information criterion (AIC; Akaike 1974). We found that the ξ values inferred by this method generally agreed with the above results, but in a few cases the results of the AIC and F test differed by 1. Note, however, that the change of ξ by 1 did not have large influence on the η estimation (e.g., $\Delta\eta < 1\%$ for $\Delta\xi = 1$) as long as the model describes the profile adequately; we included this small variation as the systematic uncertainty.

The best-fit functions are displayed in Figure 2. Note that the estimated η value varies depending weakly on the number of bins. To mitigate this variation, we changed the number of bins by ~10%, regarded the standard deviation of η as a systematic uncertainty and added it to the statistical one. These systematic uncertainties are comparable to the statistical ones.

Note that we could not determine $\dot{P}$ for any of the targets with our timing analysis because the observational data we analyzed covered only a short time interval (e.g., tens of ks) and thus the effect of $\dot{P}$ was indiscernible. For this reason, we use P and $\dot{P}$ values reported in the McGill magnetar catalog for the correlation study (see Section 4.1).

3.3. Results of the Spectral and Timing Analyses

Here we briefly describe the spectral and temporal properties of the targets and present our measurements. Note that the errors on the parameters reported in this section are 1σ uncertainties obtained from spectral fitting (with fixed N_H unless noted otherwise).

CXOU J010043.1−721134 in the small Magellanic cloud is a persistent magnetar whose emission has been stable for approximately three decades (McGarry et al. 2005; Chatterjee et al. 2021). A previous study (Tiengo et al. 2008) of the source performed with multi-epoch data suggested that its quiescent spectrum is best described by a 2BB model with $N_H = (6.3^{+2.0}_{-1.6}) \times 10^{20}$ cm^{-2}, $kT_1 = 0.30 \pm 0.02$ keV $kT_2 = 0.68^{+0.09}_{-0.07}$ keV while other commonly used spectral models (e.g., BB+PL) were disfavored by the multi-epoch data. This magnetar's η was measured to be $32 \pm 3\%$ in the 0.2–6 keV (Tiengo et al. 2008).

We used the longest XMM data acquired on 2005 November 27, measured the quiescent spectrum, and fit it with a BB+PL and a 2BB model. It is beneficial to use low-energy (e.g., <0.5 keV) data for this source with very low N_H, and hence we fit the data in the 0.1–10 keV band as was done by Tiengo et al. (2008). We found that both spectral models adequately describe the spectrum, and the best-fit parameters are $kT_1 = 0.34 \pm 0.01$ keV and $\Gamma = 1.9 \pm 0.1$ (for $N_H = 9.1 \times 10^{20}$ cm^{-2}; Tiengo et al. 2008) for the BB+PL model, and $kT_1 = 0.29 \pm 0.02$ keV and $kT_2 = 0.57 \pm 0.07$ keV (for $N_H = 6.3 \times 10^{20}$ cm^{-2}) for the 2BB model. For this source, we use the BB+PL parameters as our baseline for the correlation study (Section 4.1), but we also consider the 2BB parameters (Section 4.2). Note that kT_2 of the 2BB model is

slightly different (but within the uncertainty) from the previously reported value; this seems to be caused by the covariance between the BB temperature and radius. Our fit favors a smaller kT_2 and a larger $R_{2,\mathrm{BB}}$. We verified that this difference did not have significant influence on the correlation results. We measured η to be $27 \pm 4\%$ in the 0.5–10 keV band.

4U 0142+61 is an old ($\tau_c = 68$ kyr), bright, and relatively stable magnetar (Rea et al. 2007a; Tendulkar et al. 2015), albeit with small and infrequent activities (e.g., Göğüş et al. 2017; Archibald et al. 2017; Coti Zelati et al. 2018). Gonzalez et al. (2010) analyzed multiple observations spread over 2000 d and suggested that the source's quiescent spectrum is mildly variable and is best described by 2BB+PL. The authors reported ranges of the spectral parameters: $kT_1 = 0.27$–0.31 keV, $kT_2 = 0.50$–0.60 keV, and $\Gamma = 2.6$–3.0 for $N_\mathrm{H} = (7.0 \pm 0.2) \times 10^{21}$ cm^2.

We selected the observation made with XMM on 2003 January 24 when the source was faintest. Because the MOS data were taken with the timing mode, we used only the PN data. Our 2BB+PL fit of the spectrum resulted in $kT_1 = 0.30 \pm 0.01$ keV, $kT_2 = 0.55 \pm 0.02$ keV, and $\Gamma = 2.90 \pm 0.04$, which are consistent with the previous measurements. The simpler BB+PL and 2BB models could be rejected statistically. The magnetar's η is known to be small (Figure 2), and we found $\eta = 7.4 \pm 0.5\%$ in the 0.5–10 keV band, which is consistent with a previous result of $7.7 \pm 0.9\%$ in the 0.3–10 keV band (e.g., Göhler et al. 2005).

SGR 0418+5729 is a low-B ($B_\mathrm{S} = 6 \times 10^{12}$ G) magnetar that was discovered due to its dramatic outburst on 2009 June 5 (Rea et al. 2013). The source flux had declined during the subsequent years and reached a quiescent level ∼2 yr after the onset of the outburst. Rea et al. (2013) analyzed long-term data spanning 3 yrs, fit the quiescent spectrum with a simple BB model having $N_\mathrm{H} = (1.15 \pm 0.06) \times 10^{21}$ cm^{-2} and $kT = 0.32 \pm 0.05$ keV, and measured η to be ∼60–80% in the 0.5–10 keV band.

We analyzed the most sensitive XMM data taken on 2012 August 25. The source spectrum was well fit with a BB model having $kT_1 = 0.36 \pm 0.02$ keV, and additional spectral components were statistically unnecessary. The source's pulsations with $\eta = 65 \pm 9\%$ were well detected.

SGR 0501+4516 underwent an outburst in 2008 (MJD 54701; 2008 August 23) and its flux decayed to a flat level ∼1 yr after the outburst (Camero et al. 2014). To measure the quiescent emission properties, Rea et al. (2009) analyzed archival ROSAT data collected between 1992 September 21 and 24 (before the 2008 outburst), and measured the 0.1–2.4 keV spectrum to be a BB ($kT = 0.38^{+0.36}_{-0.15}$ keV) or a PL ($\Gamma > 0.6$) for $N_\mathrm{H} = 6^{+5}_{-3} \times 10^{21}$ cm^{-2} with the 1–10 keV observed fluxes of 1.3×10^{-12} erg cm^{-2} s^{-1} and 4.2×10^{-12} erg cm^{-2} s^{-1} for the BB and PL model, respectively. On the other hand, Mong & Ng (2018) performed a spectral analysis with multi-epoch data spread over ∼5 yrs ('post-burst' Chandra and Suzaku data taken between 2008 and 2013) and found that a BB+PL model with $kT_1 = 0.63^{+0.04}_{-0.05}$ keV, $\Gamma = 3.9^{+0.3}_{-0.2}$ for $N_\mathrm{H} = (1.43^{+0.09}_{-0.08}) \times 10^{22}$ cm^{-2}, or a 2BB+PL model with

$kT_1 = 0.26^{+0.01}_{-0.02}$ keV, $kT_2 = 0.62^{+0.03}_{-0.04}$ keV and $\Gamma = 2.3^{+0.7}_{-2.5}$ for $N_\mathrm{H} = (9.0 \pm 0.2) \times 10^{21}$ cm^{-2} fits the data well; they favored the latter based on some high-energy residuals.

The source fluxes measured by Mong & Ng (2018) are higher by ∼50% than that measured with ROSAT, possibly indicating that the source had not returned to its quiescent state or that the source's quiescent emission is variable. We, however, speculated that this discrepancy might be caused by ROSAT's lack of >2 keV sensitivity. To confirm this, we used two Chandra observations taken on 2012 December 9 and 2013 April 3 when the source flux decreased by an order of magnitude compared to the maximum (see Camero et al. 2014). For a spectral analysis we restricted the energy band to '0.5–2.4 keV' to compare with the ROSAT results and held N_H fixed at 6×10^{21} cm^{-2} which was used for the ROSAT analysis (see above). We found out that the 'Chandra' spectra are well modeled with a BB having $kT = 0.39 \pm 0.01$ keV with the 1–10 keV observed flux of 1.4×10^{-12} erg cm^{-2} s^{-1}. These results are in good agreement with the ROSAT measurements, meaning that the magnetar actually returned to the preburst state at the epoch of the Chandra observations.

Our analysis of the aforementioned Chandra data in the '0.5–10 keV' band ruled out the simple BB model, and thus we used BB+PL, 2BB and 2BB+PL models (e.g., Mong & Ng 2018) and found that the PL component of the 2BB+PL model is statistically unnecessary. The best-fit parameters for the BB+PL model are $kT_1 = 0.74 \pm 0.04$ keV and $\Gamma = 3.9 \pm 0.1$, and those for the 2BB model are $kT_1 = 0.27 \pm 0.01$ keV and $kT_2 = 0.72 \pm 0.02$ keV. Our best-fit BB temperatures do not agree well with those of Mong & Ng (2018). This discrepancy is presumably induced by parameter covariance; holding kT_2 and Γ fixed at their values in our fits reproduces their results. Note also that they jointly analyzed the Chandra and Suzaku data (2013 August), whereas we used only the Chandra data. We verified that this difference in kT_2 did not have a significant impact on the correlation results (Section 4). We use our best-fit BB+PL model for the correlation study, but also consider the 2BB and 2BB+PL models (Section 4.2). We measured $\eta = 46 \pm 2\%$ (0.5–10 keV), which is consistent with $45 \pm 6\%$ in the 0.3–12 keV band measured when the source was slightly brighter (with 2009 XMM data; Camero et al. 2014).

SGR 0526−66 was discovered in the supernova remnant (SNR) N49 in the large Magellanic cloud (LMC). The source exhibited a giant flare in 1979 (Cline et al. 1982) but no strong activity has been seen since then. Güver et al. (2012) found that the source flux has decreased slowly by ∼20–30% over 15 yrs by comparing 1994 ROSAT (Rothschild et al. 1994), 2000/2001 and 2009 Chandra measurements; no significant change of the BB temperature was seen. Given the small flux decay rate, we assumed that the source has been in (near) a quiescent state over the 15-yr period. A previous spectral analysis of multi-epoch data found that a BB+PL or a 2BB model adequately explains the observed spectrum (Park et al. 2012). The best-fit parameters inferred from the analysis are $N_\mathrm{H,Gal} = 6 \times 10^{20}$ cm^{-2} (Galactic absorption), $N_\mathrm{H,LMC} = (5.44^{+0.58}_{-0.59}) \times 10^{21}$ cm^{-2} (LMC absorption), $kT_1 = 0.44 \pm 0.02$ keV, and $\Gamma = 2.5^{+0.11}_{-0.12}$ for the BB+PL model,

and $N_{\rm H,Gal} = 6 \times 10^{20}$ cm^{-2}, $N_{\rm H,LMC} = 1.70^{+0.25}_{-0.23} \times 10^{21}$ cm^{-2}, $kT_1 = 0.39 \pm 0.01$ keV, and $kT_2 = 1.01^{+0.11}_{-0.09}$ keV for the 2BB model. Note that the authors favored the 2BB model because the fit-inferred $N_{\rm H,LMC}$ towards the magnetar agrees better with that inferred towards the surrounding SNR. Pulsations of this magnetar were only weakly detected, and the reported η values are diverse; Tiengo et al. (2009) measured it to be $13.6 \pm 0.9\%$ in the 0.65–12 keV band, whereas Güver et al. (2012) reported η of 1.5–4.4% in the 0.5–6.5 keV band. The discrepancy might be caused by different definitions of η and energy bands used for the measurements.

We used the Chandra data acquired on 2009 September 19 when the source flux was lowest (see Güver et al. 2012). For an analysis of the Chandra data, we adopted the BB+PL and 2BB models and found $kT_1 = 0.45 \pm 0.03$ keV and $\Gamma = 2.4 \pm 0.1$ (BB+PL), and $kT_1 = 0.40 \pm 0.02$ keV and $kT_2 = 1.0 \pm 0.1$ keV (2BB), using the corresponding absorption column densities reported by Park et al. (2012) for each of the spectral models. We use the BB+PL parameters for the correlation study, but also consider the 2BB ones (Section 4.2). The source pulsations were not well detected in the Chandra data and so we could not reliably measure η for this source.

1E 1048.1−5937 is a bright magnetar that has exhibited frequent outbursts and bursts (e.g., Gavriil & Kaspi 2004; An et al. 2014; Archibald et al. 2020). Its quiescent state was well identified by long-term monitoring (e.g., Tam et al. 2008; Archibald et al. 2020), and Tam et al. (2008) analyzed Chandra monitoring observations taken in a stable and quiescent state. They found that a BB+PL model with $N_{\rm H} = (0.97 \pm 0.01) \times 10^{22}$ cm^{-2}, $kT_1 = 0.50$–0.56 keV, and $\Gamma = 2.72$–3.14 describes the source spectra well, and that η is 61–70% in the 2–10 keV band (see also Yang et al. 2016).

We analyzed the Chandra data taken on 2006 September 23, fit the spectrum with a BB+PL model, and found the best-fit parameters to be $kT_1 = 0.57 \pm 0.01$ keV and $\Gamma = 3.0 \pm 0.1$. The source pulsations were well detected and η was measured to be $68 \pm 1\%$ in the 0.5–10 keV band.

1E 1547.0−5408 is a radio magnetar (i.e., radio pulsations; Gelfand & Gaensler 2007; Camilo et al. 2007) that underwent an outburst in 2007 (e.g., Halpern et al. 2008). The source was in the lowest flux state in 2006 just before the outburst (Bernardini et al. 2011). The authors analyzed multi-epoch data taken in outburst (in 2009) and in quiescent (in 2006), fit the quiescent spectrum with a BB+PL model, and measured $kT_1 = 0.43 \pm 0.03$ keV, $\Gamma = 4.0 \pm 0.2$, and $N_{\rm H} = (3.46 \pm 0.03) \times 10^{22}$ cm^{-2}. Note that the $N_{\rm H}$ value was inferred from a joint fit of the multiple-epoch data. In the quiescent data, Bernardini et al. (2011) did not detect significant pulsations and hence reported an upper limit of ≤15% for η.

We also analyzed the XMM data collected on 2006 August 21 and were able to rule out single component models (BB or PL). For the BB+PL model, we measured the best-fit parameters to be $kT_1 = 0.40 \pm 0.02$ keV and $\Gamma = 4.0 \pm 0.1$. Our search for the 2-s pulsations resulted in an insignificant detection in agreement with Bernardini et al. (2011) (see also Gelfand & Gaensler 2007).

SGR 1627−41 has shown outbursts in 1998 and 2008 (e.g., Kouveliotou et al. 1998, 2003; Esposito et al. 2008). Although a 'stable' flux state of the source could not be convincingly identified in a long-term light curve (An et al. 2018), the source flux reached a historical minimum in 2015, ≥2000 d after the latest outburst; we assumed that the magnetar was in quiescence at that time. The source spectrum measured with the 2015 XMM data was modeled by a $\Gamma = 2.0 \pm 0.3$ PL (An et al. 2018) for $N_{\rm H} = (1.0 \pm 0.2) \times 10^{23}$ cm^{-2} (Esposito et al. 2008).

We analyzed the 2015 XMM data and found $\Gamma = 2.1 \pm 0.3$ for $N_{\rm H} = 10^{23}$ cm^{-2}. A BB model also achieves a good fit with $N_{\rm H} = (7 \pm 3) \times 10^{22}$ cm^{-2} and $kT_1 = 1.2 \pm 0.1$ keV, but the temperature appears to be too high compared to those of other quiescent magnetars. So we do not consider the BB model in our correlation study. Its pulsations were detected only during an outburst (bright) state (Esposito et al. 2008), and the 2015 XMM data were not sufficient for a detection of the pulsations. Note that the correlation results did not change much whether or not we included this source.

CXOU J164710.2−455216 is a low-B magnetar possibly associated with the star cluster Westerlund 1 and has a characteristic age of ~Myr (Muno et al. 2006). It was in a stable low-flux ('quiescent') state with the 2–10 keV flux of $(2$–$3) \times 10^{-13}$ erg cm^{-2} s^{-1} (An et al. 2013a; Coti Zelati et al. 2018) before MJD 54000 when the source underwent an outburst. Muno et al. (2007) fit XMM data taken on 2006 September 16 (MJD 53995; a week before the outburst) with a BB model and inferred kT_1 to be 0.54 ± 0.01 keV (for $N_{\rm H} = 1.28 \times 10^{22}$ cm^2), but a joint analysis of long-term data (including the XMM data of Muno et al. 2007) suggested that a BB+PL model with $N_{\rm H} = (2.39 \pm 0.05) \times 10^{22}$ cm^{-2}, $kT_1 = 0.59 \pm 0.06$ keV and $\Gamma = 3.86 \pm 0.22$ explains the spectrum better (An et al. 2013a).

We analyzed the XMM data taken on MJD 53995 and found that a BB+PL model with $kT_1 = 0.56 \pm 0.05$ keV and $\Gamma = 3.8 \pm 0.2$ explains the data adequately. A simple BB model could be ruled out with an F-test probability of 4×10^{-9}. Although the pulsations of the source were well detected, η of the source measured with the XMM data has not been reported previously. We detected its pulsations with high significance and measured the pulsed fraction to be $\eta = 80 \pm 3\%$. Note that $\dot{P}$ for this magnetar has been controversial (Rodríguez Castillo et al. 2014) but a recent study carried out with NICER data found $\dot{P} \approx 2 \times 10^{-13}$ (An & Archibald 2019). We reported this value in Table 2.

1RXS J170849.0−400910 is a very bright magnetar whose emission was detected >100 keV (Kuiper et al. 2006). This magnetar has not exhibited any outburst, and its flux seems mildly (~50%) variable (Şaşmaz Muş & Göğüş 2013; Rea et al. 2007b). A previous analysis of ~10 yr data found that the source's quiescent spectrum is well described by a BB+PL model having $kT_1 = 0.41$–0.48 keV, $\Gamma = 2.5$–2.8, and $N_{\rm H} = (1.36 \pm 0.04) \times 10^{22}$ cm^{-2}, and that η is $35.4 \pm 0.5\%$ in the 0.3–8 keV band (Rea et al. 2007b).

We used the Chandra observation taken on 2004 July 3 when the source had the lowest flux. We fit the source spectrum with a BB+PL model and measured the best-fit parameters to

be $kT_1 = 0.455 \pm 0.004$ keV and $\Gamma = 2.50 \pm 0.02$ which are within the ranges of the previous estimations. The spectral fit was acceptable with the null hypothesis probability of 0.1, but some residual trends are noticeable at low energies (Figure 1). Note that the observation was taken with the CC mode and thus an accurate estimation of the background was difficult, which might cause the residual. Its 11-s pulsations were significantly detected and η was measured to be $32.4 \pm 0.5\%$ in our analysis. **CXOU J171405.7−381031** is a bright 3.8-s magnetar associated with the SNR CTB 37B (Halpern & Gotthelf 2010). The source has been stable for ∼10 yrs without exhibiting any burst or outburst since the Chandra discovery in 2010. Gotthelf et al. (2019) jointly analyzed XMM/PN and NuSTAR data taken on 2016 September 22–23, fit the spectrum with a BB+PL model having $N_H = (3.6 \pm 0.5) \times 10^{22}$ cm^{-2}, $kT_1 = 0.62 \pm 0.04$ keV and $\Gamma = 0.9 \pm 0.3$ (90% confidence interval). They measured η to be $44 \pm 4\%$ in the 1–5 keV band.

We analyzed the same XMM data (MOS+PN) and were able to reproduce the previous results: $kT_1 = 0.61 \pm 0.01$ keV and $\Gamma = 0.9 \pm 0.4$. The pulsations of the source were detected with high significance, and we measured $\eta = 29 \pm 3\%$ in the 0.5–10 keV band. This is slightly lower than the previous measurement of $44 \pm 4\%$; the discrepancy may stem from the different energy bands as this magnetar shows a change of the pulse profile with energy (Gotthelf et al. 2019).

Note that Γ we inferred from the XMM data varies substantially (by $\Delta\Gamma = 0.4$; Table 1) when we varied N_H within its 68% uncertainty. This Γ uncertainty can be significantly reduced by jointly analyzing NuSTAR hard X-ray data as was done by Gotthelf et al. (2019). We therefore jointly analyzed the XMM (PN+MOS) and NuSTAR (Obs. ID 30201031002) observations, and were able to better constrain both N_H and Γ to within 1.3×10^{21} cm^{-2} and 0.1, respectively. Nonetheless, we use the large uncertainty ($\Delta\Gamma = 0.4$) for our simulations (i.e., for $\langle\kappa_{1,2}\rangle$; see Section 4) to be conservative. Note that the best-fit parameters do not change in our joint analysis of the XMM and NuSTAR data and hence the correlation results (i.e., $\kappa_{1,2}$; see Section 4) do not alter.

SGR 1806−20 is one of the few magnetars that have exhibited a giant flare (2004 December 27.; Hurley et al. 2005; Mereghetti et al. 2005; Terasawa et al. 2005). The source flux has been low and stable since 2010, which establishes well the quiescent state of the source (Younes et al. 2017; Coti Zelati et al. 2018). Its quiescent emission (after 2010) was slightly lower than a preburst level (i.e., before 2004; Younes et al. 2015), and was well characterized by a BB+PL model with $kT_1 = 0.59$–0.67 keV, $\Gamma = 1.27$–1.38, and $N_H = (10 \pm 3) \times 10^{22}$ cm^{-2} (2015–2016 NuSTAR data; Younes et al. 2017). These are consistent with results of the multi-epoch XMM data analysis (Younes et al. 2015) which constrained N_H better $((9.7 \pm 0.1) \times 10^{22}$ cm$^{-2})$. The root-mean-square (RMS) η of the source was measured to be 3–8% over the 8 yrs between 2003 and 2011 (Younes et al. 2015).

Because the BB emission can be more accurately measured with XMM than NuSTAR, we analyzed the 2011 XMM data to characterize the quiescent emission of the source. Note

that we did not use the MOS2 data because they were taken with the timing mode. We fit the XMM spectrum with a BB+PL model and found $kT_1 = 0.59 \pm 0.03$ and $\Gamma = 1.4 \pm 0.1$ (for $N_H = 9.7 \times 10^{22}$ cm^{-2}; Younes et al. 2015). Although the source is bright at X-rays, the detection significance for its pulsations in the quiescent data was modest because of the low η (e.g., Woods et al. 2007) which we measured to be $6 \pm 2\%$. **XTE J1810−197** was serendipitously discovered on 2003 July 15 during its relaxation into a quiescent state after an undetected outburst between 2002 November 17 and 2003 January 23 (Ibrahim et al. 2004). The source flux in 2003 was higher by approximately two orders of magnitude compared to the historical minimum measured by ROSAT in 1991–1993 (Gotthelf et al. 2004). Analyses of the ROSAT survey data suggested that the preburst spectrum of the source is well described with a BB model having $kT_1 = 0.18 \pm 0.02$ keV and the 0.5–10 keV absorbed flux of $(5.5$–$8.3) \times 10^{-13}$ erg cm^{-2} s^{-1} for $N_H = 6.3 \times 10^{21}$ cm^{-2} (Gotthelf et al. 2004), or a 2BB model having $kT_1 = 0.16 \pm 0.03$ keV, $R_{1,BB} = 16 \pm 5$ km, $kT_2 = 0.26 \pm 0.06$ keV and $R_{2,BB} < 5$ km for $N_H = (7.5 \pm 0.8) \times 10^{21}$ cm^{-2} (Bernardini et al. 2009). The source flux seemed to have reached the stationary preburst level since 2007 (Alford & Halpern 2016; Pintore et al. 2019). The lowest flux state after the outburst was observed by Chandra on 2014 March 1 (a decade after the outburst), and Vurgun et al. (2019) fit the source spectrum with a 2BB model, inferring $N_H = (9.2 \pm 0.2) \times 10^{21}$ cm^{-2}, $kT_1 = 0.18 \pm 0.01$ keV and $kT_2 = 0.36 \pm 0.01$ keV.

We reanalyzed the 2014 Chandra data, measured the source spectrum, and fit it with a BB+PL or 2BB model. The best-fit BB+PL parameters are $kT_1 = 0.32 \pm 0.03$ keV, $\Gamma = 7 \pm 1$ for $N_H = (1.7 \pm 0.2) \times 10^{22}$ cm^{-2}, and the 2BB parameters are $kT_1 = 0.17 \pm 0.01$ keV and $kT_2 = 0.33 \pm 0.02$ keV (for $N_H = 9.2 \times 10^{21}$ cm^{-2}; Vurgun et al. 2019). Note that we optimized N_H for the BB+PL model because it has not been explored previously. The PL index inferred from the BB+PL model is uncomfortably large. Presumably, it is an artifact caused by forcing to fit high-temperature BB emission with the PL model. For this reason, the 2BB model has been favored over the BB+PL one for this source (e.g., Gotthelf et al. 2004; Alford & Halpern 2016). We, therefore, use the 2BB parameters for the correlation study (Section 4.1). We estimated η to be $33 \pm 3\%$ in the 0.5–10 keV band, which is slightly lower than $41 \pm 5\%$ measured in the 1.5–5 keV band (Alford & Halpern 2016).

Note that the 0.5–10 keV absorbed flux of 8.3×10^{-13} erg cm^{-2} s^{-1} and kT_2 inferred from the 2BB fit are slightly higher than but within the uncertainties of the ROSAT measurements. This may indicate some variability. Alternatively, it may mean that the Chandra data do not represent very well the quiescent state of the source. Hence we also investigate the correlations with the ROSAT-measured spectral parameters (Section 4.2) and verified that the results did not alter significantly.

Swift J1822.3−1606 is a faint low-B magnetar (Scholz et al. 2014; Rodríguez Castillo et al. 2016) that was discovered in

outburst on 2011 July 14 (Cummings et al. 2011; Livingstone et al. 2011). The source flux has decreased since then and seemed to have reached a stationary level ~1000 d after the onset of the outburst (Coti Zelati et al. 2018). A 'preburst' spectrum of the source measured with archival ROSAT data collected in 1993 was fit with a BB model having $kT = 0.12 \pm 0.02$ keV and an absorbed 0.1–2.4 keV flux of $9^{+20}_{-9} \times 10^{-14}$ erg cm^{-2} s^{-1} for $N_{\rm H} = (4.53 \pm 0.08) \times 10^{21}$ cm^{-2} (Scholz et al. 2012). Note that this $N_{\rm H}$ value was inferred from a joint fit of multi-epoch Swift and Chandra data with a BB+PL model. The ROSAT data were not sensitive enough to allow a detection of the pulsations. Scholz et al. (2012) therefore used Swift observations taken when the source was slightly brighter than at the ROSAT epoch and measured η to be 45–50% in the 2–10 keV band.

To measure the 'post-burst' quiescent spectrum, Mong & Ng (2018) analyzed five Chandra observations taken between 2014 April 14 and 2014 October 11, and reported the best-fit parameters of a 2BB model of $kT_1 = 0.11 \pm 0.01$ keV and $kT_2 = 0.29 \pm 0.03$ keV for $N_{\rm H} = (6.2 \pm 0.5) \times 10^{21}$ cm^{-2}. We also analyzed the five Chandra observations and fit the source spectra with a BB+PL or 2BB model. These models explain the observed spectra equally well, and the best-fit parameters for the BB+PL model are $kT = 0.12 \pm 0.01$ keV and $\Gamma = 4.6 \pm 0.4$ (for $N_{\rm H} = 4.53 \times 10^{21}$ cm^{-2}; Scholz et al. 2014), and those for the 2BB model are $kT_1 = 0.11 \pm 0.01$ keV and $kT_2 = 0.27 \pm 0.02$ keV (for $N_{\rm H} = 6.2 \times 10^{22}$ cm^{-2}; Mong & Ng 2018).

To compare with the ROSAT results, We tried to fit the 0.1–2.4 keV Chandra spectrum with a simple BB model. The Chandra data required an additional model component, and the measured 0.1–2.4 keV absorbed flux of 1.7×10^{-13} erg cm^{-2} s^{-1} is ~2 times higher than (but within the uncertainty of) the ROSAT measurement. This may indicate some variability of the quiescent flux or alternatively suggest that the source did not reach the quiescent state (e.g., ROSAT measured state) in 2014. Although the large uncertainties in the ROSAT measurements preclude a firm conclusion, the differences are not large, meaning that the source was in or 'near' quiescence. Thus, we use the Chandra BB+PL parameters as our baseline for the correlation study, but investigate the correlations with the ROSAT-measured properties as well (Section 4.2). The source's pulsations were well detected in the Chandra data, and we measured η to be 38 ± 3%.

1E 1841−045 is the power source of the SNR Kes 73 and is the first magnetar from which >100 keV emission was discovered (Molkov et al. 2004). It has not shown a dramatic outburst, but hard X-ray bursts have been detected (e.g., An et al. 2015). The source emission is very strong and stable in the X-ray band, and so its quiescent spectrum was relatively well measured; Morii et al. (2003) and An et al. (2013b) fit the spectrum with a BB+PL model and found the best-fit parameters to be $kT = 0.42$–0.44 keV and $\Gamma = 2.0$–2.1 for $N_{\rm H} = (2.2$–$2.3) \times 10^{22}$ cm^{-2}.

We measured the source spectrum using the XMM data taken on 2002 October 7, fit the spectrum with a BB+PL model,

and obtained the best-fit parameters of $kT = 0.41 \pm 0.01$ keV and $\Gamma = 2.2 \pm 0.1$ (for $N_{\rm H} = (2.26 \pm 0.05) \times 10^{22}$ cm^{-2}; An et al. 2013b). The source's pulsations were well detected, and the measured η is 15 ± 2%, which is consistent with 19 ± 3% in the 0.6–7 keV band (Morii et al. 2003).

SGR 1900+14 is a magnetar that exhibited a giant flare (1998 August 27; Feroci et al. 1999). The source flux appears to have reached a quiescent level since 2006 (Mereghetti et al. 2006; Tamba et al. 2019). Tamba et al. (2019) fit quiescent spectra measured by XMM and NuSTAR with a BB+PL model having $kT = 0.52^{+0.02}_{-0.01}$ keV, $\Gamma = 1.4 \pm 0.3$, and $N_{\rm H} = (1.9 \pm 0.1) \times 10^{22}$ cm^{-2}, and measured η to be 19–22% in the 1–10 keV band.

We analyzed the XMM data taken on 2016 October 20 (the XMM data analyzed by Tamba et al. 2019) when the source flux was lowest. The XMM spectra were well fit with a BB+PL model having $kT = 0.52 \pm 0.01$ keV and $\Gamma = 1.3 \pm 0.2$, and η was measured to be 20 ± 2% in the 0.5–10 keV band.

1E 2259+586 is a bright magnetar within the SNR CTB 109, and exhibited outbursts in 2002 (Kaspi et al. 2003) and 2014–2016. A long-term light curve (Zhu et al. 2008) showed that the source flux has declined relatively rapidly to a quiescence level on a timescale of a few years. Woods et al. (2004) measured a quiescent spectrum of the magnetar using the XMM observation taken on 2002 January 22, just before the 2002 outburst, and reported the best-fit BB+PL parameters of $kT = 0.49 \pm 0.01$ keV, and $\Gamma = 4.04 \pm 0.08$ for $N_{\rm H} = (1.10 \pm 0.02) \times 10^{22}$ cm^{-2}.

We analyzed the same XMM data that Woods et al. (2004) used and fit the spectrum with a BB+PL model. Note that we used only the PN data because the MOS data are severely affected by the pile-up effect (Woods et al. 2004). The best-fit BB+PL parameters are $kT = 0.48 \pm 0.02$ keV and $\Gamma = 4.03 \pm 0.05$. The pulsations of the source were detected with high significance and η was measured to be 18 ± 1% which is consistent with a previous measurement of 23 ± 5% in the 2–10 keV band (Woods et al. 2004; Zhu et al. 2008).

4. Correlation Analysis

4.1. Correlation Study with the Baseline Model Parameters

We grouped the magnetars' properties into timing and emission properties for a cross-correlation study. The six timing properties, P and $\dot{P}$, $B_{\rm S}$, $\dot{E}_{\rm SD}$, τ_c, and $\dot{\nu}$ are all derived from two measured parameters: P and $\dot{P}$. The number of emission properties differs for each spectral model (Table 2), but we used the following 9 properties: kT_1, $R_{1,\rm BB}$, $L_{\rm BB}$ ($= L_{1,\rm BB} + L_{2,\rm BB}$), Γ, PL flux ($F_{\rm PL}$), PL luminosity $L_{\rm PL}$, total X-ray luminosity $L_{\rm X}$ ($= L_{\rm BB} + L_{\rm PL}$), a distance independent luminosity ratio $\zeta = L_{\rm PL}/L_{\rm BB}$, and η. Note again that $F_{\rm PL}$, $L_{\rm PL}$, η, and ξ were measured in the 0.5–10 keV band.

We constructed 54 temporal-emission property pairs and 36 emission-emission property pairs. Since power-law relations between some properties have been predicted by magnetar models, we employed a log scale for the properties except

Table 2. Significantly correlated property pairs

Properties		κ_1^a (σ)	$\langle\kappa_1\rangle^a$ (σ)	$\sigma_{\kappa 1}^b$ (σ)	κ_2^a (σ)	$\langle\kappa_2\rangle^a$ (σ)	$\sigma_{\kappa 2}^b$ (σ)
$\dot{P}$	L_{BB}	3.3	3.2	0.3	3.3	3.3	0.3
$\dot{P}$	Γ	−3.4	−3.4	0.4	−2.5	−2.6	0.3
$\dot{P}$	L_X	3.3	3.0	0.3	3.2	2.9	0.3
B_S	L_{BB}	3.6	3.5	0.3	3.6	3.7	0.4
B_S	Γ	−3.6	−3.5	0.5	−2.7	−2.7	0.4
B_S	L_X	3.7	3.4	0.3	3.6	3.3	0.3
τ_c	L_{BB}	−3.0	−2.9	0.3	−3.0	−3.0	0.3
τ_c	Γ	3.1	3.1	0.4	2.2	2.3	0.2
$R_{1,BB}$	L_{BB}	4.2	4.2	0.3	4.1	4.0	0.3
$R_{1,BB}$	L_X	3.0	2.9	0.3	2.9	2.8	0.3
$R_{1,BB}$	ζ	−3.4	−2.8	0.5	−1.8	−1.4	0.5
L_{BB}	L_{PL}	3.9	4.0	0.4	2.5	2.7	0.5
L_{BB}	L_X	6.5	6.3	0.4	6.5	6.3	0.4
F_{PL}	L_{PL}	2.1	2.2	0.3	3.9	3.6	0.9
F_{PL}	L_X	1.8	1.9	0.3	3.1	3.0	0.7
L_{PL}	L_X	7.4	7.7	0.6	5.5	6.0	0.6

[a]Correlation significance in units of σ. Negative values mean anti-correlation.
[b]Variation of the correlation significance due to uncertainties on the properties. See text for more details

Table 3. 2BB parameters for some magnetars

Name	Model	kT_1 (keV)	$R_{1,BB}$ (km)	kT_2 (keV)	$R_{2,BB}$ (km)
J0100	2BB	0.29(2)	12(1)	0.57(7)	2(1)
SGR0501	2BB	0.27(1)	1.5(1)	0.72(2)	0.15(1)
SGR0526	2BB	0.40(2)	11(1)	1.0(1)	1.2(4)
J1822	2BB	0.11(1)	6(1)	0.27(2)	0.3(1)

emission properties were anticipated from the constructions of the quantities (e.g., $L_X = L_{BB} + L_{PL}$), but the $R_{1,BB}$-L_{BB}, and L_{BB}-L_{PL} correlations are intriguing. The $R_{1,BB}$-ζ correlation is also intriguing, but it is induced by a few high-ζ points with very large uncertainties (Figure 4) and thus varies significantly (e.g., $\sigma_{\kappa 1}$ and κ_2 in Table 2). Hence this correlation is rather uncertain.

4.2. Correlation Study with Alternative Spectral Models

In Section 4.1, we used the spectral parameters of the baseline models reported in Table 1 (mostly BB+PL). However, 2BB models have also been suggested and favored for some magnetars on statistical or physical grounds (see Section 3.3). These targets are listed in Table 3. We replaced the BB+PL spectral parameters with the 2BB ones for these targets and computed the correlation significances (κ_2; Table 2). We also performed 10,000 simulations as was done is Section 4.1, and measured average correlation significances ($\langle\kappa_2\rangle$) and standard deviations ($\sigma_{\kappa 2}$). The results are reported in Table 2.

The significantly-correlated properties found using the baseline models mostly remain unchanged, but some of the PL-related correlations ($\dot{P}$-Γ, B_S-Γ, and L_{BB}-L_{PL}) became less significant when the 2BB parameters were used perhaps because of the reduction in the number of PL samples. Notice that those PL-related correlations are still modest (e.g., $|\kappa_2| \geq 2.5$ except for the τ_c-Γ correlation). Correlations with the higher-temperature BB properties ($R_{2,BB}$ and $L_{2,BB}$) could not be measured due to the lack of 2BB samples.

5. Discussion

We presented a refined list of quiescent magnetars and investigated correlations between their spectral and temporal properties, including η which has not been explored previously. We further considered uncertainties in the spectral and temporal parameters as well as the distances to the targets using simulations. Hence, our correlation study is more thorough than the previous ones. Here we discuss some intriguing correlations (e.g., $|\kappa_1| \gtrsim 3$; Section 4.1) obtained using the baseline models (Table 1). Using 2BB models for some of the targets (Section 4.2) alters significances of PL-related correlations as noted above.

5.1. Significant Correlations between Temporal and Emission Properties

As noted in Section 4.1, the timing properties are derived from P and $\dot{P}$ measurements, and then the correlations of the emis-

for Γ, η, and ζ (see also Kaspi & Boydstun 2010; Enoto et al. 2010; An et al. 2012; Mong & Ng 2018). Scatter plots of the property pairs are displayed in Figures 3 and 4. For each pair of the properties, we computed the Pearson's correlation coefficient and used the Fisher transformation (Fisher 1915) to estimate the correlation significance (κ_1). Property pairs with $|\kappa_1| \geq 3.0$ or $|\kappa_2| \geq 3.0$ (Section 4.2), and their correlation significances are presented in Table 2.

Note that it is difficult to accurately measure P and $\dot{P}$ of magnetars because of large timing noise and glitches. Moreover, distances (d's) to magnetars are poorly constrained. Thus there are various suggestions for those values.[5] In general, the suggested values of P for a magnetar differ only little ($\Delta P/P \leq 10^{-2}$), which is not a concern for the correlation study. However, those of $\dot{P}$ (and d) are substantially different. To take this into account, we performed simulations. For each target, we randomly picked a $\dot{P}$ and a d (uniform priors) value among the suggested ones, and further varied the spectral parameters. Note that the spectral parameters are known to covary, and the covariance was taken into account in the simulations as follows. We varied N_H using the value and uncertainty presented in Table 1. We held N_H fixed at the varied value and refit the spectral data to derive the best-fit spectral parameters appropriate for the varied N_H. We then used the covariance matrix provided by XSPEC to generate a simulated set of the spectral parameters for each target, and computed the correlation coefficients. We repeated this procedure 10,000 times and measured the mean ($\langle\kappa_1\rangle$) and standard deviation ($\sigma_{\kappa 1}$); these are presented in Table 3 for reference.

The timing properties $\dot{P}$ and B_S are well correlated with the emission properties L_{BB}, Γ and L_X. τ_c also shows correlations with L_{BB} and Γ. Some correlations between the

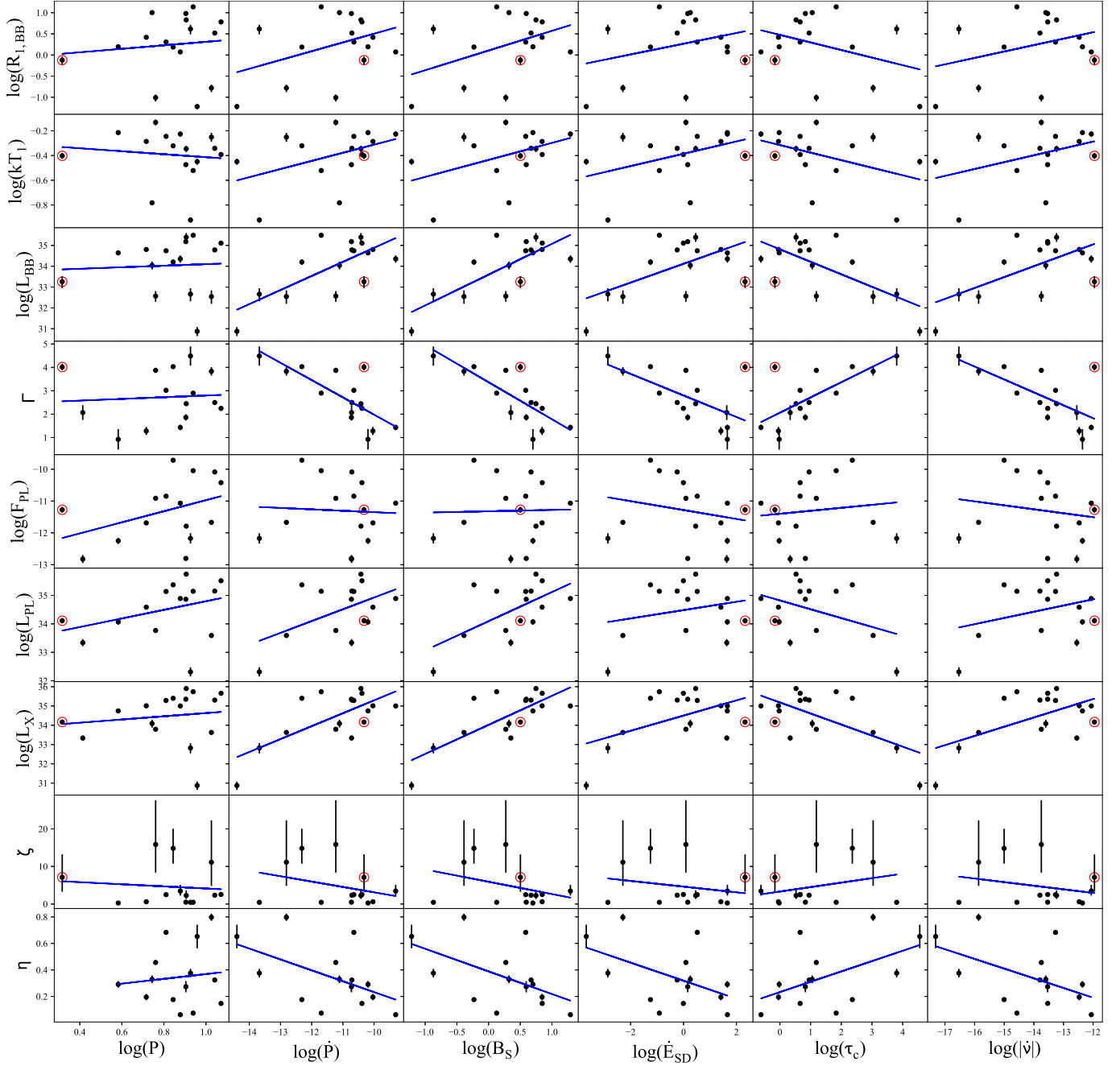[5]http://www.physics.mcgill.ca/~pulsar/magnetar/TabO2.html

Figure 3. Scatter plots of the emission and temporal properties. Least-square fits of the correlation trends with linear functions are displayed in blue for reference. Parameters for the magnetar 1E 1547.0−5408 are denoted by red circles (see Section 5.1).
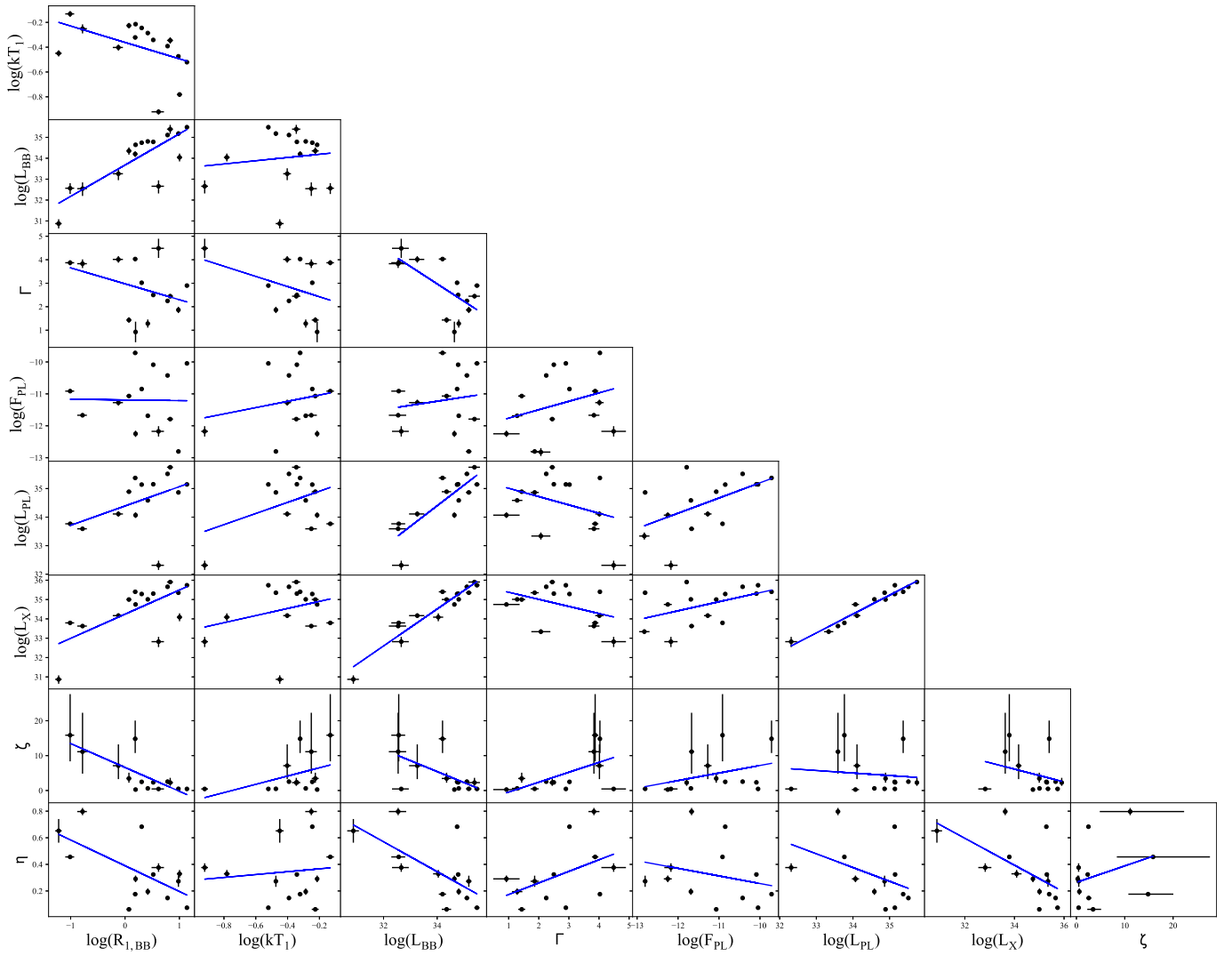
Figure 4. Scatter plots of the emission properties. The best-fit linear functions are displayed in blue for reference.

sion properties with $\dot{P}$ (Table 2) might have induced those with the other timing properties that are combinations of P and $\dot{P}$ (e.g., B_S and τ_c). The timing properties are thought to represent physical quantities approximately, and the results (Table 3) show that there are better (or worse) combinations of P and $\dot{P}$ that make the correlations more (less) significant. These can provide insights into magnetars' evolution and emission mechanisms (e.g., Marsden & White 2001; Kaspi & Boydstun 2010; An et al. 2012; Mong & Ng 2018).

The results presented in Table 2 confirm the previously suggested B_S-Γ (Kaspi & Boydstun 2010) and B_S-L_X (An et al. 2012; Mong & Ng 2018) correlations. The B_S-Γ (anti-)correlation has been explained as due to an increased optical depth to the RCS in high-B sources (Thompson et al. 2002); photons make multiple scattering and the magnetospheric particles have larger velocity spread, rendering the soft nonthermal spectrum harder (e.g., Fernández & Thompson 2007; Kaspi & Boydstun 2010). For the B_S-L_X correlation, we further separately investigated the thermal (L_{BB}) and nonthermal (L_{PL}) luminosities, and found that B_S is significantly correlated with L_{BB} and not with L_{PL} ($\kappa_1 = 2.4$). This indicates that the

B_S-L_X correlation is mainly driven by the B_S-L_{BB} one. We speculate that this may be because L_{BB} is directly affected by the B decay, whereas L_{PL} is influenced by both L_{BB} (seeds for RCS) and magnetospheric current (scatterer for RCS). Hence the B_S-L_{PL} correlation might have been blurred. The B_S-L_X correlation supports the idea that magnetars' emission power is supplied primarily by the internal B decay for which magnetar models predict $L_X \propto B^{4.4}$ (original magnetar model; Thompson & Duncan 1996) or $L_X \propto B$ (twisted-B model; Thompson et al. 2002). In our fit of the B_S-L_X trend (Figure 3), we found $L_X \propto B_S^{1.5}$ (and $L_{BB} \propto B_S^{1.5}$). While the spin-inferred B_S's may not accurately represent true B's of magnetars, if assuming so, the result seems to agree reasonably with the twisted-B model.

We discovered intriguing correlations of τ_c with L_{BB} and Γ. These correlations are expected as magnetars lose their internal B energy via long-term cooling; L_{BB} drops and the nonthermal (RCS) emission softens with time. Theoretically, Thompson & Duncan (1996) predicted $L_{BB} \propto t^{-0.3}$–$t^{-0.4}$ and a recent magneto-thermal evolution model predicted diverse trends depending on the initial configuration of B (e.g., Figure 7

of Viganò et al. 2013). To compare with the model predictions, we fit the τ_c-L_{BB} trend with a power-law function and found $L_{BB} \propto \tau_c^{-0.6}$. It appears to agree reasonably well with the theoretical predictions of Thompson & Duncan (1996) and Viganò et al. (2013).

Marsden & White (2001) suggested a possible correlation between the spin-down torque ($\dot{\nu}$) and Γ using a small sample (7 magnetars). Kaspi & Boydstun (2010) investigated this correlation using a larger sample (11 magnetars) and noted that the $\dot{\nu}$-Γ correlation is significant only at 1.8σ which increases to 2.7σ when ignoring 1E 1547.0−5408 for which the Γ measurement was very uncertain (i.e., $\Gamma = 3.7^{+0.8}_{-2.0}$; Gelfand & Gaensler 2007). Later Bernardini et al. (2011) refined the Γ measurement ($\Gamma = 4.0 \pm 0.2$) using multi-epoch data. Hence we did not exclude 1E 1547.0−5408 from our correlation study (15 magnetars) and found a modest correlation between $\dot{\nu}$ and Γ at 2.8σ. This correlation is certainly intriguing but is not yet definitive. Related to the $\dot{\nu}$-Γ correlation, we found that the spin-down 'rate' $\dot{P}$ ($-\frac{\dot{\nu}}{\nu^2}$) is better correlated with Γ. This correlation is in accordance with the twisted-B model of magnetars (Thompson et al. 2002) which predicted that the twist increases the current flowing across the light cylinder, thereby resulting in an increase of the spin-down rate and the optical depth; the latter makes the spectrum harder (i.e., smaller Γ).

1E 1547.0−5408 seems to be an outlier for the Γ-related correlations (Figure 3) as was noted by Kaspi & Boydstun (2010) for the $\dot{\nu}$-Γ correlation. Ignoring it from the sample makes all the Γ-related correlations stronger. We note that the property pairs of the source, except for the Γ-related ones, lie close to the correlation trends (Figure 3), meaning that the source has properties of typical magnetars but its nonthermal emission is very soft. It is intriguing to note that the other target XTE J1810−197 also shows extremely soft PL ($\Gamma = 7$) emission for its rotational properties, if we consider the BB+PL model for the source (Section 3.3). Magnetospheric X-ray emission of these targets seems to be highly suppressed despite their strong $>10^{14}$ G field. This may be related to the fact that the two magnetars 1E 1547.0−5408 and XTE J1810−197 are the few 'radio magnetars' in which pulsed radio signals have been detected (only two in our target list; see also Chu et al. 2021). This is only speculative, and further studies are needed to address this issue.

5.2. Correlation between B_S and kT

As we showed above (Section 5.1), B_S has significant influence on BB emissions of magnetars. Then, kT_{BB} may also be correlated with B_S. However, we did not find any significant correlation between them ($\kappa_1 = 1.7$). Note that Pons et al. (2007) discovered a B_S-kT_{BB} correlation in a sample of 'isolated neutron stars' with B_S in the range of 10^{12}–10^{15} G (i.e., including some thermally emitting X-ray pulsars and magnetars). They further measured the correlation trend to be $kT_{BB} \propto B_S^{0.5}$ and suggested that the correlation implies that the internal heat is generated by magnetic field decay: $B_S^2 \propto T_{BB}^4$. However, it appears that the correlation in the magnetar group alone seemed insignificant in that work (Figure 1 of Pons et al.

2007), and Zhu et al. (2011) noted that the B_S-kT_{BB} correlation is insignificant in a larger sample of neutron stars (normal pulsars, high-B pulsars, and X-ray-isolated neutron stars) than was used by Pons et al. (2007). These mean that the B_S-kT_{BB} correlation suggested by Pons et al. (2007) might be caused by clustering of the pulsars (low B_S and kT_{BB}) and the magnetars (high B_S and kT_{BB}): i.e., a correlation between the pulsar and the magnetar populations not within the "isolated neutron star" population.

In the magnetar population, Rea et al. (2008), using a physically-motivated RCS model, found no significant correlation between the surface temperature (kT) and B_S. On the other hand, Mong & Ng (2018) used a 2BB or a 2BB+PL model for a sample of magnetars, and suggested that the model-inferred temperature for the cooler BB emission with a radius greater than 3 km is correlated with B_S ($kT_{BB} \propto B_S^{0.4}$). So the current situation for the B_S-kT_{BB} correlation in the magnetar population is unclear as the correlation significance alters substantially depending on the spectral model and targets used for the studies. Further theoretical and observational studies are warranted.

5.3. Correlations between Emission Properties

We found significant correlations in a number of emission property pairs (Table 2 and Figure 4), which can provide hints to emission mechanisms of magnetars as compared to RPPs. As we noted above, both magnetars and RPPs emit nonthermal X-ray radiation in the magnetosphere, but suggested emission mechanisms are very different: RCS off of the thermal seed photons (i.e., L_{BB}) for magnetars *vs* synchrotron radiation for RPPs. While the RCS scenario has been favored over the synchrotron scenario for magnetars based on theoretical arguments and observed spectral features (e.g., spectral turn-over at $\gtrsim 10$ keV in some magnetars), further observational supports would help to discern the scenarios more clearly. A difference between the RCS and synchrotron scenarios is that the nonthermal emission is strongly affected by the thermal one as the latter provides seeds for the former in the RCS scenario, whereas the thermal and nonthermal emissions are not strongly related to each other in the synchrotron scenario. Hence, the correlation we found between L_{BB} and L_{PL} supports the RCS scenario for magnetar's nonthermal emission.

The $R_{1,BB}$-$L_{1,BB}$ (and $R_{1,BB}$-L_X) correlation is observationally obvious as $L_{BB} \propto R_{BB}^2 kT_{BB}^4$. In this case, however, the lack of L_{BB}-kT_{BB} correlation ($\kappa_1 = 0.4$) is puzzling. This is probably because the simple BB+PL or 2BB model only approximately represents magnetars' emission. For example, some low-energy contamination from multiple cold spots and/or magnetosphere might be ascribed to the BB model, which would increase the fit-inferred $R_{1,BB}$ and L_{BB} but lower kT_{BB}, thereby enhancing the $R_{1,BB}$-L_{BB} correlation and blurring the kT_{BB}-L_{BB} one.

5.4. Comparisons with Other Neutron-Star Populations

Correlations of the emission and temporal properties in the populations of RPPs with nonthermal X-ray emission (Li et al.

2008) and thermally emitting pulsars (Zhu et al. 2011) have also been studied. Li et al. (2008) carried out a correlation study with temporal and 'nonthermal' emission properties of 27 RPPs. Although only some of the property pairs are correlated with high significance (e.g., chance probabilities of $p < 10^{-3}$), it appears that the RPPs' nonthermal X-ray luminosity $L_{\mathrm{X,psr}}$ is well correlated with their temporal properties P, $\dot{P}$, τ_c, and $\dot{E}_{\mathrm{SD}}$, and X-ray photon index Γ is reasonably well correlated with P and $\dot{E}_{\mathrm{SD}}$. Neither $L_{\mathrm{X,psr}}$ nor Γ was found to be correlated with B_S; we confirmed this by reanalyzing the data presented in Li et al. (2008). Recalling that magnetars' Γ and L_X are correlated with B_S but not with $\dot{E}_{\mathrm{SD}}$ (Table 2), the two populations, magnetars and RPPs, seem to be very different. This supports the idea that the primary energy sources of magnetars and RPPs are different; B for the former and the rotational energy for the latter.

On the other hand, Zhu et al. (2011) investigated correlations of 'thermal' emission properties with temporal ones using a sample of thermally emitting pulsars (high-B pulsars, normal pulsars and X-ray-isolated neutron stars; see Zhu et al. 2011, for more detail). Because the authors considered only B_S-kT correlation, we reanalyzed the data (kT, R_{BB}, and L_{BB}) presented in Zhu et al. (2011) after supplementing them with P and $\dot{P}$ taken from the ATNF catalog[6], and found out that L_{BB} is correlated with τ_c at the 3σ level. Again, neither L_{BB} nor kT is significantly correlated with $\dot{E}_{\mathrm{SD}}$ or B_S having significances $<2\sigma$. This may indicate that cooling of these thermally emitting pulsars occurs primarily by release of the residual heat in the core, not by the spin down or a B decay. The cooling trend of the sources is measured to be $L_{\mathrm{BB}} \propto \tau_c^{-0.47}$. These pulsars seem to cool relatively slowly compared to magnetars ($L_{\mathrm{BB}} \propto \tau_c^{-0.6}$), meaning that magnetars' energy loss (by B and residual heat) is larger than the thermally emitting pulsars'.

In summary, these comparisons suggest that thermal and nonthermal emissions of the pulsars (i.e., RPPs and thermally emitting pulsars) arise from residual heat and spin-down energy, respectively, whereas magnetars' emission is strongly affected by the decay of B. While there are more to be studied by analyzing emission and temporal properties of the neutron-star populations (i.e., magnetars, RPPs, and the thermally emitting pulsars) simultaneously, we defer such a research to future work, since we need to scrutinize the measurements made for the pulsars (e.g., Li et al. 2008; Zhu et al. 2011) presumably by reanalyzing the data as we did here for magnetars.

6. Summary

- We found that the emission properties, the thermal luminosity L_{BB} and the X-ray photon index Γ, are correlated with the spin-down rate ($\dot{P}$), the surface dipole magnetic field strength (B_S) and characteristic age τ_c.

- We found $L_{\mathrm{BB}} \propto B_S^{1.5}$ and $L_{\mathrm{BB}} \propto \tau_c^{-0.6}$ trends which are similar to predictions of magnetar models.

- We found that L_{BB} is correlated with L_{PL}. This correlation supports the RCS scenario for magnetars' nonthermal

---

[6] https://www.atnf.csiro.au/research/pulsar/psrcat/

emission.

- The correlations in the magnetar population are different from those seen in other neutron-star populations (e.g., RPPs and thermally emitting pulsars), indicating that the energy sources for emissions of magnetars and the other neutron stars are different.

While the results obtained from our study suggest intriguing correlations that can help to delineate emission mechanisms in magnetars, there are things to be improved. While the spectral models we used in this work seem to represent the thermal and nonthermal properties of magnetars well, some residuals are noticeable (Figure 1), possibly suggesting that the actual emission of magnetars may be different from these simple models. A well-justified physical model of magnetars' emissions is lacking, but a correlation study with such a model in the future may reveal different correlations among the physical properties of the stars. The current identifications of the 'quiescent' state of the targets may not be very accurate. Besides, $\dot{P}$ of some magnetars was measured during an outburst period, and in this case the measurement might be biased to a larger value by a putative glitch and its recovery (e.g., Woods et al. 2007). Better identification of the quiescent states and more accurate measurements of $\dot{P}$ can be achieved with a deeper and high-cadence monitoring campaign for the magnetars over a long period. The current/future X-ray missions eROSITA (Predehl et al. 2021), Lynx (Gaskin et al. 2019), AXIS (Mushotzky et al. 2019) and Athena (Barcons et al. 2017) will certainly be very helpful.

Some magnetars exhibit a distinct hard X-ray (e.g., ≥ 10 keV) spectrum which we did not consider because they have been accurately measured only for a small number of magnetars (e.g., Kuiper et al. 2006). The hard-band properties may be correlated with the temporal and soft-band properties (e.g., Thompson & Beloborodov 2005; Beloborodov 2013; Wadiasingh et al. 2018), and can provide further insights into magnetar physics (e.g., Kaspi & Boydstun 2010; Enoto et al. 2010; Yang et al. 2016). Deeper NuSTAR (Harrison et al. 2013) and future HEX-P (Madsen et al. 2018) observations of quiescent magnetars are warranted.

Acknowledgments

References

Akaike, H. 1974, IEEE Transactions on Automatic Control, 19, 716

Alford, J. A. J., & Halpern, J. P. 2016, ApJ, 818, 122

An, H., & Archibald, R. 2019, ApJ, 877, L10

An, H., Cumming, A., & Kaspi, V. M. 2018, ApJ, 859, 16

An, H., Kaspi, V. M., Archibald, R., & Cumming, A. 2013a, ApJ, 763, 82

An, H., Kaspi, V. M., Tomsick, J. A., et al. 2012, ApJ, 757, 68

An, H., Hascoët, R., Kaspi, V. M., et al. 2013b, ApJ, 779, 163

An, H., Kaspi, V. M., Beloborodov, A. M., et al. 2014, ApJ, 790, 60

An, H., Archibald, R. F., Hascoët, R., et al. 2015, ApJ, 807, 93

Anders, E., & Grevesse, N. 1989, Geochim. Cosmochim. Acta, 53, 197

Archibald, R. F., Kaspi, V. M., Scholz, P., et al. 2017, ApJ, 834, 163

Archibald, R. F., Kaspi, V. M., Tendulkar, S. P., & Scholz, P. 2018, ApJ, 869, 180

Archibald, R. F., Scholz, P., Kaspi, V. M., Tendulkar, S. P., & Beardmore, A. P. 2020, ApJ, 889, 160

Arnaud, K. A. 1996, in Astronomical Society of the Pacific Conference Series, Vol. 101, Astronomical Data Analysis Software and Systems V, ed. G. H. Jacoby & J. Barnes, 17

Barcons, X., Barret, D., Decourchelle, A., et al. 2017, Astronomische Nachrichten, 338, 153

Beloborodov, A. M. 2009, ApJ, 703, 1044

Beloborodov, A. M. 2013, ApJ, 762, 13

Beloborodov, A. M., & Thompson, C. 2007, ApJ, 657, 967

Bernardini, F., Israel, G. L., Dall'Osso, S., et al. 2009, A&A, 498, 195

Bernardini, F., Israel, G. L., Stella, L., et al. 2011, A&A, 529, A19

Bochenek, C. D., Ravi, V., Belov, K. V., et al. 2020, Nature, 587, 59

Camero, A., Papitto, A., Rea, N., et al. 2014, MNRAS, 438, 3291

Camilo, F., Ransom, S. M., Halpern, J. P., & Reynolds, J. 2007, ApJ, 666, L93

Chatterjee, R., Agrawal, V. K., & Nandi, A. 2021, MNRAS, 505, 3785

CHIME/FRB Collaboration, Amiri, M., Bandura, K., et al. 2018, ApJ, 863, 48

CHIME/FRB Collaboration, Andersen, B. C., Bandura, K. M., et al. 2020, Nature, 587, 54

Chu, C.-Y., Ng, C. Y., Kong, A. K. H., & Chang, H.-K. 2021, MNRAS, 503, 1214

Cline, T. L., Desai, U. D., Teegarden, B. J., et al. 1982, ApJ, 255, L45

Coti Zelati, F., Rea, N., Pons, J. A., Campana, S., & Esposito, P. 2018, MNRAS, 474, 961

Şaşmaz Muş, S., & Göğüş, E. 2013, ApJ, 778, 156

Cummings, J. R., Burrows, D., Campana, S., et al. 2011, The Astronomer's Telegram, 3488, 1

de Jager, O. C., Raubenheimer, B. C., & Swanepoel, J. W. H. 1989, A&A, 221, 180

Enoto, T., Nakazawa, K., Makishima, K., et al. 2010, ApJ, 722, L162

Esposito, P., Israel, G. L., Zane, S., et al. 2008, MNRAS, 390, L34

Fernández, R., & Thompson, C. 2007, ApJ, 660, 615

Feroci, M., Frontera, F., Costa, E., et al. 1999, ApJ, 515, L9

Fisher, R. A. 1915, Biometrika, 10, 507

Gaskin, J., Özel, F., Vikhlinin, A., & Swartz, D. 2019, Journal of Astronomical Telescopes, Instruments, and Systems, 5, 021000

Gavriil, F. P., Gonzalez, M. E., Gotthelf, E. V., et al. 2008, Science, 319, 1802

Gavriil, F. P., & Kaspi, V. M. 2004, ApJ, 609, L67

Gelfand, J. D., & Gaensler, B. M. 2007, ApJ, 667, 1111

Göhler, E., Wilms, J., & Staubert, R. 2005, A&A, 433, 1079

Goldreich, P., & Reisenegger, A. 1992, ApJ, 395, 250

Gonzalez, M. E., Dib, R., Kaspi, V. M., et al. 2010, ApJ, 716, 1345

Gotthelf, E. V., Halpern, J. P., Buxton, M., & Bailyn, C. 2004, ApJ, 605, 368

Gotthelf, E. V., Halpern, J. P., Mori, K., & Beloborodov, A. M. 2019, ApJ, 882, 173

Göğüş, E., Lin, L., Roberts, O. J., et al. 2017, ApJ, 835, 68

Güver, T., Göğüş, E., & Özel, F. 2012, MNRAS, 424, 210

Halpern, J. P., & Gotthelf, E. V. 2010, ApJ, 710, 941

Halpern, J. P., Gotthelf, E. V., Reynolds, J., Ransom, S. M., & Camilo, F. 2008, ApJ, 676, 1178

Harrison, F. A., Craig, W. W., Christensen, F. E., et al. 2013, ApJ, 770, 103

Ho, W. C. G. 2016, MNRAS, 463, 489

Ho, W. C. G., & Lai, D. 2001, MNRAS, 327, 1081

Hurley, K., Boggs, S. E., Smith, D. M., et al. 2005, Nature, 434, 1098

Ibrahim, A. I., Markwardt, C. B., Swank, J. H., et al. 2004, ApJ, 609, L21

Kaspi, V. M., & Beloborodov, A. M. 2017, ARA&A, 55, 261

Kaspi, V. M., & Boydstun, K. 2010, ApJ, 710, L115

Kaspi, V. M., Gavriil, F. P., Woods, P. M., et al. 2003, ApJ, 588, L93

Kouveliotou, C., Kippen, M., Woods, P., et al. 1998, IAU Circ., 6944, 2

Kouveliotou, C., Eichler, D., Woods, P. M., et al. 2003, ApJ, 596, L79

Kuiper, L., Hermsen, W., den Hartog, P. R., & Collmar, W. 2006, ApJ, 645, 556

Li, X.-H., Lu, F.-J., & Li, Z. 2008, ApJ, 682, 1166

LIGO Scientific Collaboration, Aasi, J., Abbott, B. P., et al. 2015, Classical and Quantum Gravity, 32, 074001

Livingstone, M. A., Scholz, P., Kaspi, V. M., Ng, C. Y., & Gavriil, F. P. 2011, ApJ, 743, L38

Loredo, T. J. 1992, in Statistical Challenges in Modern Astronomy, 275–297

Lyutikov, M. 2003, MNRAS, 346, 540

Lyutikov, M., & Gavriil, F. P. 2006, MNRAS, 368, 690

Madsen, K. K., Harrison, F., Broadway, D., et al. 2018, in Society of Photo-Optical Instrumentation Engineers (SPIE) Conference Series, Vol. 10699, Space Telescopes and Instrumentation 2018: Ultraviolet to Gamma Ray, ed. J.-W. A. den Herder, S. Nikzad, & K. Nakazawa, 106996M

Marsden, D., & White, N. E. 2001, ApJ, 551, L155

McGarry, M. B., Gaensler, B. M., Ransom, S. M., Kaspi, V. M., & Veljkovic, S. 2005, ApJ, 627, L137

Mereghetti, S., Götz, D., von Kienlin, A., et al. 2005, ApJ, 624, L105

Mereghetti, S., Esposito, P., Tiengo, A., et al. 2006, ApJ, 653, 1423

Molkov, S. V., Cherepashchuk, A. M., Lutovinov, A. A., et al. 2004, Astronomy Letters, 30, 534

Mong, Y. L., & Ng, C. Y. 2018, ApJ, 852, 86

Morii, M., Sato, R., Kataoka, J., & Kawai, N. 2003, PASJ, 55, L45

Muno, M., Gaensler, B., Clark, J. S., et al. 2006, The Astronomer's Telegram, 902, 1

Muno, M. P., Gaensler, B. M., Clark, J. S., et al. 2007, MNRAS, 378, L44

Mushotzky, R., Aird, J., Barger, A. J., et al. 2019, in Bulletin of the American Astronomical Society, Vol. 51, 107

Olausen, S. A., & Kaspi, V. M. 2014, ApJS, 212, 6

Park, S., Hughes, J. P., Slane, P. O., et al. 2012, ApJ, 748, 117

Perna, R., & Pons, J. A. 2011, ApJ, 727, L51

Pintore, F., Mereghetti, S., Esposito, P., et al. 2019, MNRAS, 483, 3832

Pons, J. A., Link, B., Miralles, J. A., & Geppert, U. 2007, Phys. Rev. Lett., 98, 071101

Potekhin, A. Y., & Yakovlev, D. G. 2001, A&A, 374, 213

Predehl, P., Andritschke, R., Arefiev, V., et al. 2021, A&A, 647, A1

Protassov, R., van Dyk, D. A., Connors, A., Kashyap, V. L., & Siemiginowska, A. 2002, ApJ, 571, 545

Rea, N., Zane, S., Turolla, R., Lyutikov, M., & Götz, D. 2008, ApJ, 686, 1245

Rea, N., Nichelli, E., Israel, G. L., et al. 2007a, MNRAS, 381, 293

Rea, N., Israel, G. L., Oosterbroek, T., et al. 2007b, Ap&SS, 308, 505

Rea, N., Israel, G. L., Turolla, R., et al. 2009, MNRAS, 396, 2419

Rea, N., Israel, G. L., Pons, J. A., et al. 2013, ApJ, 770, 65

Regimbau, T., & de Freitas Pacheco, J. A. 2006, ApJ, 642, 455

Rodríguez Castillo, G. A., Israel, G. L., Esposito, P., et al. 2014, MNRAS, 441, 1305

Rodríguez Castillo, G. A., Israel, G. L., Tiengo, A., et al. 2016, MNRAS, 456, 4145

Rothschild, R. E., Kulkarni, S. R., & Lingenfelter, R. E. 1994, Nature, 368, 432

Scholz, P., Kaspi, V. M., & Cumming, A. 2014, ApJ, 786, 62

Scholz, P., Ng, C. Y., Livingstone, M. A., et al. 2012, ApJ, 761, 66

Tam, C. R., Gavriil, F. P., Dib, R., et al. 2008, ApJ, 677, 503

Tamba, T., Bamba, A., Odaka, H., & Enoto, T. 2019, PASJ, 71, 90

Tendulkar, S. P., Hascöet, R., Yang, C., et al. 2015, ApJ, 808, 32

Terasawa, T., Tanaka, Y. T., Takei, Y., et al. 2005, Nature, 434, 1110

Thompson, C., & Beloborodov, A. M. 2005, ApJ, 634, 565

Thompson, C., & Duncan, R. C. 1995, MNRAS, 275, 255

Thompson, C., & Duncan, R. C. 1996, ApJ, 473, 322

Thompson, C., Lyutikov, M., & Kulkarni, S. R. 2002, ApJ, 574, 332

Tiengo, A., Esposito, P., & Mereghetti, S. 2008, ApJ, 680, L133

Tiengo, A., Esposito, P., Mereghetti, S., et al. 2009, MNRAS, 399, L74

Tiengo, A., Esposito, P., Mereghetti, S., et al. 2013, Nature, 500, 312

Torres, D. F., Viganò, D., Coti Zelati, F., & Li, J. 2019, MNRAS, 489, 5494

Verner, D. A., Ferland, G. J., Korista, K. T., & Yakovlev, D. G. 1996, ApJ, 465, 487

Viganò, D., Rea, N., Pons, J. A., et al. 2013, MNRAS, 434, 123

Vogel, J. K., Hascöet, R., Kaspi, V. M., et al. 2014, ApJ, 789, 75

Vurgun, E., Chakraborty, M., Güver, T., & Göğüş, E. 2019, New A, 67, 45

Wadiasingh, Z., Baring, M. G., Gonthier, P. L., & Harding, A. K. 2018, ApJ, 854, 98

Wang, Y., Takata, J., & Cheng, K. S. 2013, ApJ, 764, 51

Woods, P. M., Kouveliotou, C., Finger, M. H., et al. 2007, ApJ, 654, 470

Woods, P. M., Kaspi, V. M., Thompson, C., et al. 2004, ApJ, 605, 378

Yang, C., Archibald, R. F., Vogel, J. K., et al. 2016, ApJ, 831, 80

Younes, G., Baring, M. G., Kouveliotou, C., et al. 2017, ApJ, 851, 17

Younes, G., Kouveliotou, C., & Kaspi, V. M. 2015, ApJ, 809, 165

Zhu, W., Kaspi, V. M., Dib, R., et al. 2008, ApJ, 686, 520

Zhu, W. W., Kaspi, V. M., McLaughlin, M. A., et al. 2011, ApJ, 734, 44